# Assemblies of Aligned Magnetotactic Bacteria and Extracted Magnetosomes: What Is the Main Factor Responsible for the Magnetic Anisotropy?

**E. Alphandéry,[†] Y. Ding,[‡] A. T. Ngo,[†] Z. L. Wang,[‡] L. F. Wu,[§] and M. P. Pileni[†,*]**

[†]Université Pierre et Marie-Curie, Laboratoire des matériaux mésoscopiques et nanométriques (LM2N), 4 place Jussieu, 75252 Paris cedex 05, France, [‡]School of Materials Science and Engineering, Georgia Institute of Technology, 500 10th Street NW, Atlanta, Georgia 30332, and [§]Laboratoire de Chimie bactérienne, IMM, CNRS, 31 Chemin Joseph Aiguier, 13402 Marseille cedex 20, France

**ABSTRACT** The origin of the magnetic anisotropy is explained in an assembly of aligned magnetic nanoparticles. For that, nanoparticles synthesized biologically by *Magnetospirillum magneticum* AMB-1 magnetotactic bacteria are used. For the first time, it is possible to differentiate between the two contributions arising from the alignment of the magnetosome easy axes and the strength of the magnetosome dipolar interactions. The magnetic anisotropy is shown to arise mainly from the dipolar interactions between the magnetosomes.

**KEYWORDS:** magnetotactic bacteria · magnetosomes · magnetic anisotropy · easy axes · dipolar interactions

Understanding the origin of the magnetic anisotropy in an assembly of aligned magnetic nanocrystals is an important challenge in the field of nanotechnology. It has implications both at a fundamental and applied level. On the one hand, it provides a deeper knowledge of the properties of organized magnetic nanocrystals. On the other hand, it helps with designing new structures useful for magnetic recording.[1,2]

It has long been known that aligning nanoparticles gives rise to magnetic anisotropy, that is, a squarer hysteresis loop for a magnetic field applied parallel to the direction of the alignment than for a magnetic field applied perpendicular to this direction. This behavior is predicted by the Stoner−Wohlfarth model[3] or more recent calculations[4] and verified experimentally by a large number of studies.[5−7] However, despite all of these studies, it has never been possible to explain clearly the origin of the magnetic anisotropy and to differentiate between the influence of the nanocrystal easy axis alignment and the dipolar interactions induced by the ordering of the nanocrystals.

To enable this distinction, we study biologically synthesized iron oxide nanoparticles, called magnetosomes, which are produced by AMB-1 magnetotatic bacteria.[8] The magnetosomes are arranged in chains inside the bacteria, creating a strong magnetic dipole, which is used by the bacteria to align and swim along the earth's magnetic field.[8] They are ferrite nanocrystals usually reported to be in their reduced ($Fe_3O_4$) form.[8] Because of oxygen exposure during the growth and sample preparation, the magnetosomes studied here are mainly made of maghemite as shown in a previous report.[9] Since magnetite and maghemite have very similar magnetic properties at room temperature, the composition of the magnetosomes in either of the two forms of the oxide would produce very similar results. The magnetostatic interactions between the magnetosomes and the biological filaments surrounding them maintain the alignment of the easy axes of the individual magnetosomes within the bacteria.[10−16] These results suggest that it is possible to extract the magnetosomes from the bacteria and obtain two types of structures, those in which the filaments are functional yielding aligned magnetosome easy axes and those lacking these filaments producing randomly distributed easy axes. In addition, the magnetosomes are large nanoparticles of mean sizes approximately equal to 30 nm with a ferromagnetic behavior at room temperature.[9] Therefore, they are prone to strong dipolar interactions.[9,17]

In this paper, we use AMB-1 magnetotactic bacteria and the magnetosomes extracted from the bacteria to explain the

*Address correspondence to pileni@sri.jussieu.fr.

Received for review March 24, 2009 and accepted May 13, 2009.

**Published online May 21, 2009.**
10.1021/nn900289n CCC: $40.75

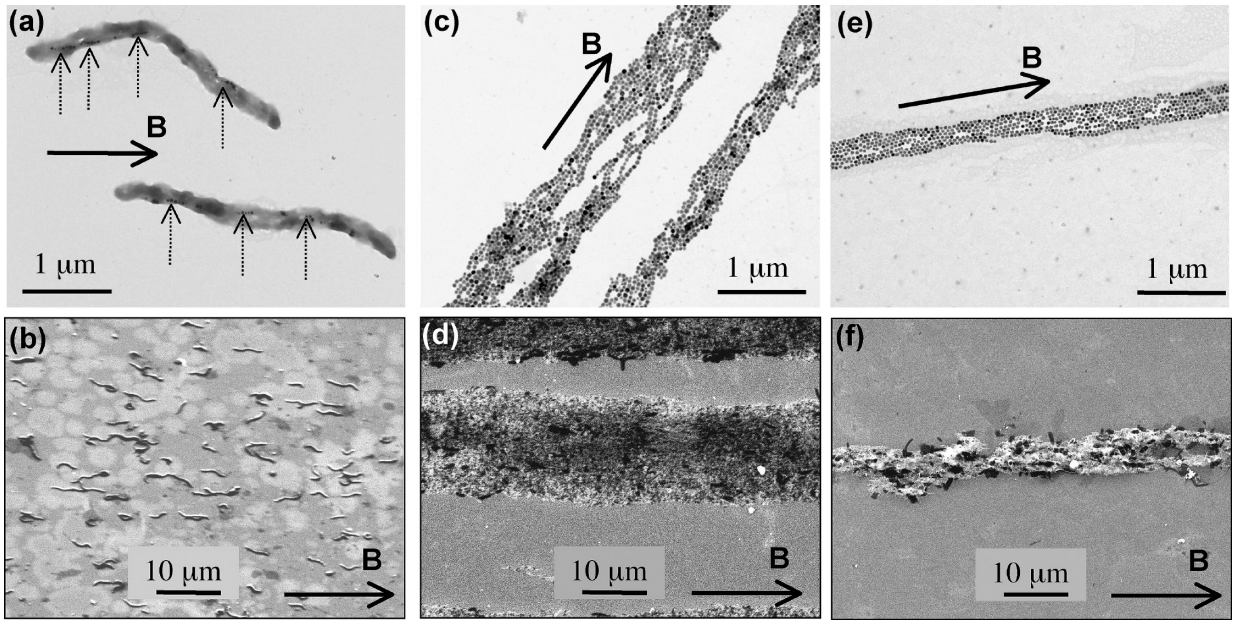


**Figure 1. TEM images of the whole magnetotactic bacteria (a), extracted unheated magnetosomes (c), and extracted SDS-treated and heated magnetosomes (e). The samples are deposited on top of a carbon grid in the presence of a magnetic field. In panel a, the dashed arrows designate the chains of magnetosomes inside the bacteria. SEM images of the whole magnetotactic bacteria (b), extracted unheated magnetosomes (d), and extracted heated and SDS-treated magnetosomes (f). The samples are deposited on top of a silicon substrate in the presence of a magnetic field. The deposition field is designated by B and the arrow below B indicates its orientation.**

origin of the magnetic anisotropy in an assembly of aligned magnetosomes. To observe the influence of the dipolar interactions on the magnetic anisotropy, we compare the behavior of the whole bacteria with that of the extracted magnetosomes. We also study the influence of the magnetosome easy axis alignment on the magnetic anisotropy. To do that, we compare the behaviors of two different types of extracted magnetosomes, those possessing the biogenic material, which aligns the easy axes of the individual magnetosomes and those lacking this material producing randomly orientated easy axes.

## RESULTS AND DISCUSSION

Let us first consider a suspension of magnetotactic bacteria containing *ca.* $2 \times 10^{-5}$ % in weight of maghemite. A 10 μL portion of this suspension is deposited on top of a transmission electron microscopy (TEM) grid covered by amorphous carbon in the presence of a 1 T magnetic field applied during the solvent evaporation. The TEM image of the magnetotactic bacteria (Figure 1a) shows that the bacteria are partially orientated in the direction of the deposition field. Each of the bacterium contains 3−4 short chains aligned in the direction of the cell long axis (designated in Figure 1a by dashed arrows). The centers of these chains are separated by more than ~0.5 μm. The distance separating two chains of magnetosomes contained in two different bacteria is more than 1 μm. The TEM grid is replaced by a silica wafer to measure the magnetic properties of the aligned bacteria. Fifty microliters of the same solution of whole bacteria are deposited on top of a silicon substrate in the presence of 1 T magnetic field. The scanning electron microscopy (SEM) image of Figure 1b shows partially aligned magnetotactic bacteria demonstrating that the partial alignment of the bacteria occurs on both substrates. To make it possible to record the magnetic responses, we use a similar sample preparation as that described above but with a larger amount of material. Fifty microliters of a more concentrated suspension of magnetotactic bacteria, containing ~$2 \times 10^{-3}$ % in weight of maghemite, are now deposited on top of a silicon substrate. Figure 2a shows that the hysteresis loop is squarer when the magnetic field is applied parallel (∥) to the aligned bacteria (green line), than when it is applied perpendicular (⊥) (red line) to this direction. For the two different field configurations, the coercive field and the reduced remanence are designated by $\mathbf{H}_{c\parallel}$, $\mathbf{H}_{c\perp}$, $(\mathbf{M}_r/\mathbf{M}_s)_{\parallel}$, and $(\mathbf{M}_r/\mathbf{M}_s)_{\perp}$, respectively. The relative changes in coercivity and reduced remanence between the two field configurations are defined as $\Delta_{\mathbf{Hc}} = (\mathbf{H}_{c\parallel} - \mathbf{H}_{c\perp})/\mathbf{H}_{c\parallel}$ and $\Delta_{\mathbf{Mr/Ms}} = ((\mathbf{M}_r/\mathbf{M}_s)_{\parallel} - (\mathbf{M}_r/\mathbf{M}_s)_{\perp})/(\mathbf{M}_r/\mathbf{M}_s)_{\parallel}$, where $\Delta_{\mathbf{Hc}}$ and $\Delta_{\mathbf{Mr/Ms}}$ measure the strength of the magnetic anisotropy. From Figure 2a, the values of $\Delta_{\mathbf{Mr/Ms}}$ and $\Delta_{\mathbf{Hc}}$ are estimated as 30% and 20%, respectively. The relatively low values of $\Delta_{\mathbf{Mr/Ms}}$ and $\Delta_{\mathbf{Hc}}$ are attributed to the rather large distance of more than 0.5 μm separating the chains of magnetosomes and to the partial alignment of the magnetosome easy axes. The large distance separating the chains of magnetosomes should result in a weakly interacting system.[18,19] We verify this result by measuring the ratio between the magnetostatic ($E_{ms}$) and anisotropy ($E_k$) energies. For this calculation, we consider

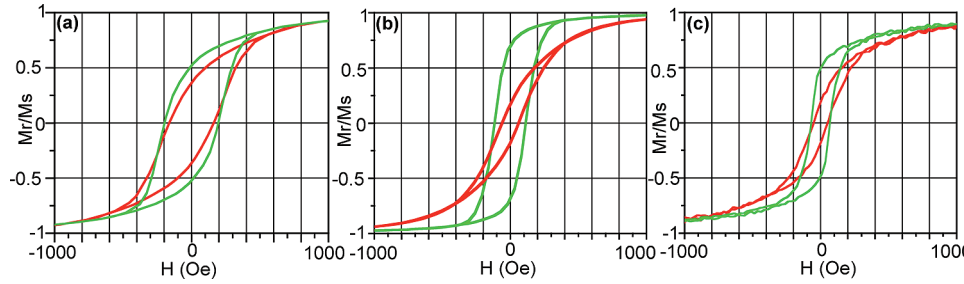


**Figure 2. Hysteresis loops of the whole magnetotactic bacteria (a), extracted unheated magnetosomes (b), and extracted heated magnetosomes (c). The magnetic field applied during the measurements of the hysteresis loops is either parallel (green line) or perpendicular (red line) to the direction of the alignment. The measurements are carried out at 300 K.**

the magnetostatic interactions between two chains of magnetosomes and the anisotropy energy of a single chain. The magnetostatic energy between two chains of magnetosomes is given by $E_{ms} = -(3\cos^2\theta - 1)(V_{ch}M_s)^2/4\pi a^3$,[20] where $V_{ch}$, $M_s$, $a$, and $\theta$ are the volume of a typical chain of magnetosomes containing six magnetosomes of mean sizes 30 nm ($16.2 \times 10^{-17}$ cm$^3$), the saturation magnetization of maghemite (390 emu/cm$^3$), the distance separating two chains of magnetosomes (2 $\mu$m), and the angle between the dipoles belonging to two different chains of magnetosomes, respectively. The schematic picture, presented in Supporting Information, shows two typical chains of magnetosomes possessing two dipoles $\mu_1$ and $\mu_2$ in interactions separated by an angle $\theta$. Since the chains of magnetosomes contained within the whole bacteria form an angle of 0 to $\pi/4$ with respect to the orientation of the deposition field, we deduce that $\theta$ lies between 0 and $\pi/4$. Using the values of $V_{ch}$, $M_s$, $a$, and $\theta$ given above, we estimate that $E_{ms}$ lies between $-10^{-15}$ erg and $-0.25 \times 10^{-15}$ erg and we deduce the mean magnetostatic energy as $\langle E_{ms}\rangle \approx -0.62 \times 10^{-15}$ erg. The anisotropy energy of a typical chain of magnetosomes is estimated as $E_k = K_{eff}V_{ch} = 194 \times 10^{-13}$ erg, where $K_{eff} \approx 12 \times 10^4$ erg/cm$^3$ is the anisotropy constant of a single magnetosome.[9] From the low value of $|\langle E_{ms}\rangle|/E_k$ ($3 \times 10^{-5}$), it is concluded that the chains of magnetosomes contained in the different bacteria are weakly interacting with each other.[21] The presence of these weak interactions combined with the partial alignment of the magnetosome easy axes is responsible for the weak magnetic anisotropy, which we observe.

To improve the alignment of the chains of magnetosomes and increase the strength of the dipolar interactions between them, the latter are extracted from the bacteria. Ten microliters of a solution of extracted magnetosomes containing $\sim 2 \times 10^{-4}$ % in weight of maghemite are now deposited on top of TEM grid in the presence of a 0.2 T magnetic field applied during the solvent evaporation. Figure 1c shows that the chains of magnetosomes orientate in the direction of the deposition field. In this case, the chains of magnetosomes organize within wide bands and form a much more compact assembly than that observed with the whole bacteria (Figure 1a). Most of the biogenic material, which belongs to the whole bacteria, is removed and the chains attract each other, forming a long string of nanoparticles. However, because of the remaining biogenic material, which binds the magnetosomes together,[22] the chains are still bent in several regions. A 50 $\mu$L portion of the same solution is deposited on top of a silicon substrate in the presence of a 0.2 T magnetic field. The SEM image of Figure 1d shows that when they are deposited on top of a silicon substrate, the extracted magnetosomes also orientate in the direction of the deposition field. To record the magnetic properties of the extracted chains of magnetosomes, 50 $\mu$L of a more concentrated suspension of extracted magnetosomes, containing $\sim 2 \times 10^{-3}$ % in weight of maghemite, are deposited on top of a silicon wafer. The hysteresis loops (Figure 2b) show a much more pronounced difference between the parallel and perpendicular configurations (green and red lines, respectively) compared to what is observed with the orientated bacteria (Figure 2a). The values of $\Delta_{M_r/M_s}$ and $\Delta_{H_c}$ are 80% and 50%, respectively, larger than $\Delta_{M_r/M_s} \approx 30\%$ and $\Delta_{H_c} \approx 20\%$ observed with the whole bacteria. To explain this behavior, we estimate the ratio between the magnetostatic and anisotropy energy in this sample. As in the whole bacteria, a dipole is associated to each chain of magnetosomes. Since the angle between the different chains of magnetosomes and the deposition field lies between 0 and $\pi/8$, we deduce that $0 < \theta < \pi/8$. Given these values of $\theta$ and a mean distance between the magnetosomes of $\sim$6 nm, the magnetostatic interaction between two chains of magnetosomes is estimated as lying between $E_{ms} \approx -3.7 \times 10^{-8}$ and $E_{ms} \approx -2.9 \times 10^{-8}$ erg. Using the values of $\langle E_{ms}\rangle \approx -3.3\ 10^{-8}$ and $E_k \approx 194 \times 10^{-13}$ erg calculated for a chain of magnetosomes, we estimate that $|\langle E_{ms}\rangle|/E_k \approx 1700$. The fact that this value is much larger than 1 indicates a strong dipolar coupling between the magnetosomes,[21] which strongly enhances the magnetic anisotropy compared with the whole bacteria. For a complete understanding of such behavior, we need to know whether or not the extraction process of the magnetosomes from the bacteria could change the orientations of their easy axes. For this purpose, high-resolution TEM experiments (HRTEM) are performed on the different types of magnetosomes and the orientations of their easy axes are identified. Since the easy axes of the magnetosomes arranged in chains have been determined to follow the $\langle 111\rangle$ crystallographic orientations,[10−13,23,24] and the crystallographic planes of the magnetosomes

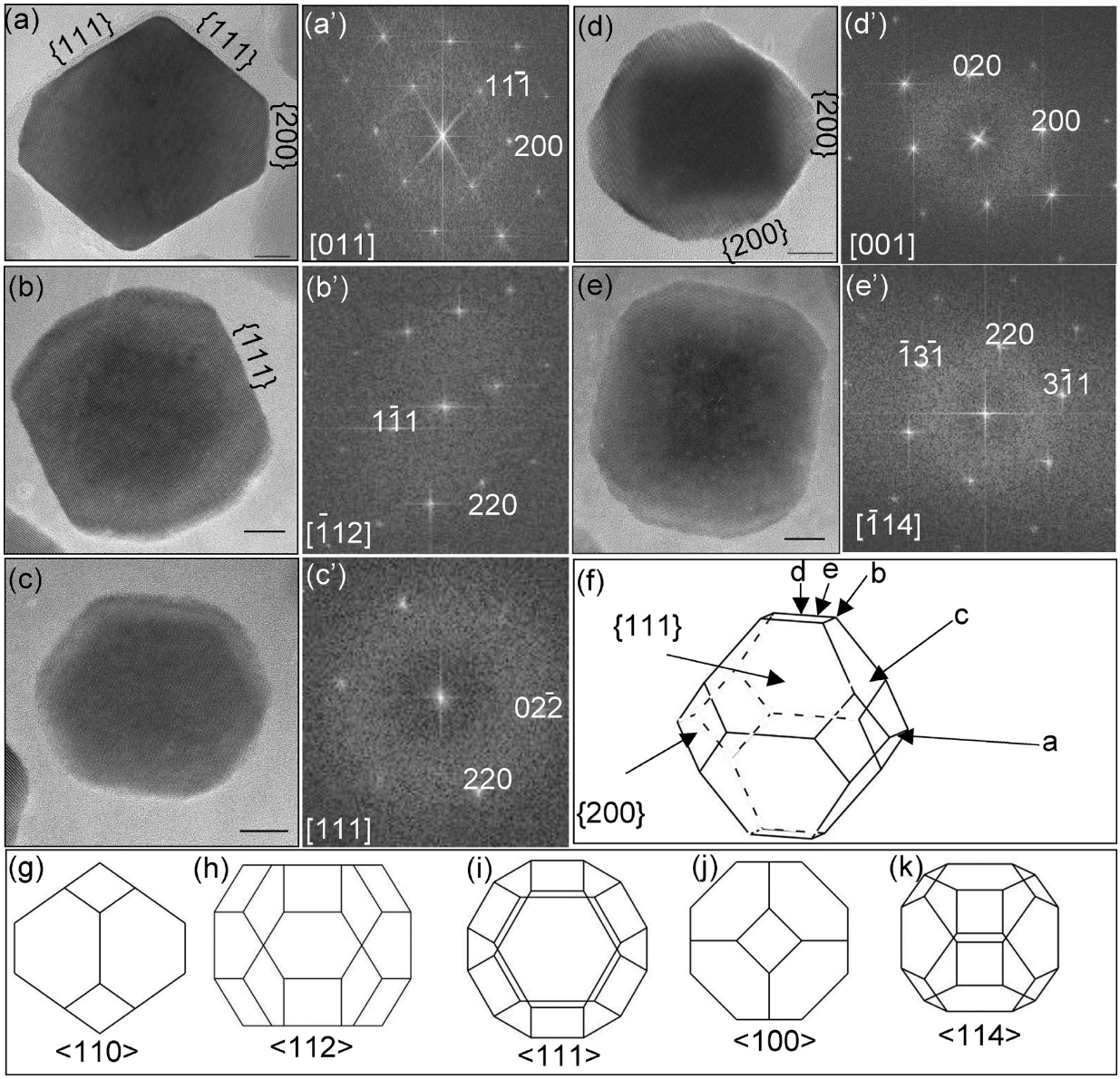


**Figure 3. HRTEM images and the corresponding diffraction patterns of magnetosomes of type I (a, a′), type II (b, b′), type III (c, c′), type IV (d, d′), type V (e, e′). (f) Schematic diagram of a cuboctahedron showing the diffraction crystallographic directions [011], [112], [111], [001], and [114]. (g−k): Schematic diagrams, which represent a typical magnetosome, having the shape of a cuboctahedron projected along ⟨110⟩ (g), ⟨112⟩ (h), ⟨111⟩ (i), ⟨100⟩ (j), ⟨114⟩ (k). The scale bar represents 10 nm.**

can be identified using HRTEM, we are able to identify the easy axis of each magnetosome using HRTEM. Figure 3a−e show the prevailing projected images of the different types of magnetosomes. The corresponding diffractograms of each HRTEM image are displayed on the right-hand side of each image. Using the symmetry of the diffractograms and the planar distance, the diffraction spots of each diffractogram are indexed. Furthermore, given that the magnetosomes have a face center cubic (fcc) structure, the incident electron beam directions in Figure 3a−e are identified as [011], [$\bar{1}$12], [$\bar{1}$11], [001], and [$\bar{1}$14], respectively. After indexing the edges of the particles in Figure 3a and Figure 3b, we find that the surface planes at the edges are either the {111} or the {200} crystallographic planes. This suggests that the magnetosomes possess the geometry of a truncated octahedron in the three-dimensional space (Figure 3f) in agreement with previous TEM studies.[25] For such a geometry, the arrows indexed by a, b, c, d, and e show the electron beam directions along the ⟨110⟩, ⟨112⟩, ⟨111⟩, ⟨001⟩, and ⟨114⟩ directions. The ideal cases of a truncated octahedron projected along ⟨110⟩, ⟨112⟩, ⟨111⟩, ⟨001⟩, and ⟨114⟩ directions are drawn in Figure 3g−k. By comparing Figure 3g−k with Figure 3a−e, we deduce that most of the magetosomes are truncated octahedra, lying on top of the substrate at different orientations. The projected images of Figure 3a−e are classified as types I, II, III, IV, and V, respectively. Our statistic results indicate that types I and II are the dominant projected images since they represent

55% and 25% of the total projected images, respectively. Since types I and II are dominant and characterized by the presence of at least one set of {111} planes, we can identify the ⟨111⟩ direction and therefore the easy axes of most of the magnetosomes simply by looking at their geometry. Figure 4a shows a HRTEM image of four magnetosomes bound *via* biogenic material. The enlarged HRTEM images from areas b and c are displayed in Figure 4b,c. From the presence of clear {111} planes, the horizontal ⟨111⟩ directions can be deduced. Figure 4d also shows a magnetosome containing a twin plane, projected right along the ⟨110⟩ direction. By identifying the twin plane to a (111) crystallographic plane (Figure 4d), the [111] crystallographic direction is identified. Figure 4a also shows that this direction follows the orientation of the chain, confirming the results obtained by electron holography, which showed that this direction was [111].[10−13] Hence, it can be concluded that the ⟨111⟩ crystallographic directions can be determined either by identifying the projected geometries or by using HRTEM measurements. In what follows, the first method will be used since it is easier. Figure 5 panels a and b show enlarged regions of Figure 1 panels a and c, respectively. The ⟨111⟩ crystallographic directions are shown using white arrows for those, which are orientated in the direction of the deposition field, that is, $\alpha < \pi/8$, and dark arrows for those that are not orientated in this direction, that is, $\alpha > \pi/8$, where $\alpha$ represents the angle between the ⟨111⟩ crystallographic directions of each individual magnetosome and the direction of the deposition field (Supporting Information, Figure 2). Both in the bacterial cells (Figure 5a) and in the extracted magnetosomes (Figure 5b), one of the ⟨111⟩ crystallographic directions of each individual magnetosome is orientated in the direction of the deposition field. From that, it is concluded that the magnetosomes inside the bacterial cells and those extracted from the bacteria both present easy axes oriented in the direction of the deposition field. Therefore, the difference in the magnetic properties observed between the whole bacteria and their extracted magnetosomes cannot be attributed to the change in the orientation of the magnetosome easy axes because it is well demonstrated that in both cases the magnetosome easy axes are orientated. The major difference between the intracellular magnetosomes and the ex-

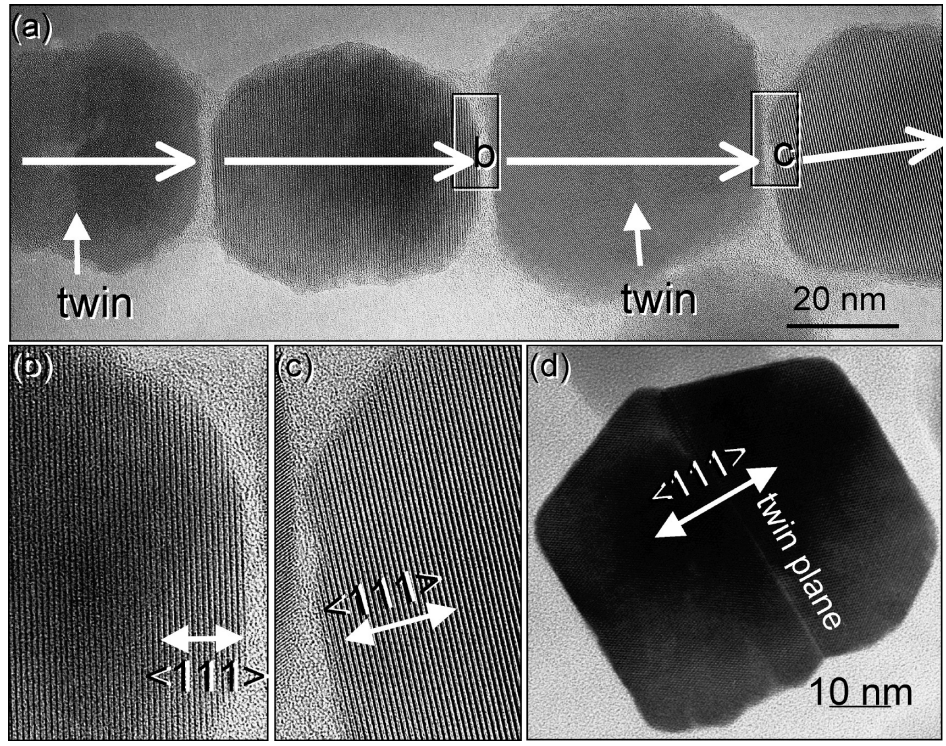


**Figure 4. (a) HRTEM image of four magnetosomes bound in a chain showing two twin crystals and two magnetososomes of type I; (b and c) enlarged regions showing the {111} diffractions plane and ⟨111⟩ crystallographic directions; (d) HRTEM image of a twin crystal, showing the twin plane and the ⟨111⟩ crystallographic orientation.**

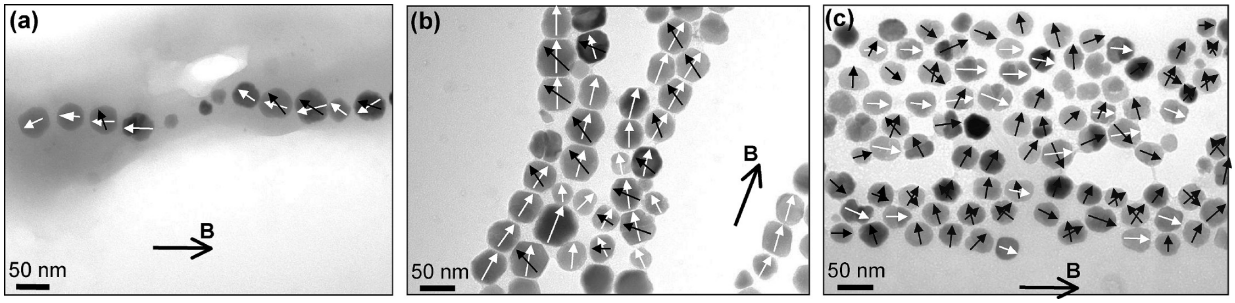


**Figure 5. (a−c) Enlarged regions of Figure 1a,c,e. The arrows indicate the ⟨111⟩ crystallographic orientations. The deposition field is designated by B and the arrow below B indicates its orientation as in Figure 1. White arrows are used when the ⟨111⟩ crystallographic orientations follow the direction of deposition field, while black arrows are used when these orientations do not follow this direction. In several magnetosomes, it is not possible to identify the ⟨111⟩ crystallographic orientations. Therefore, there is no arrow.**

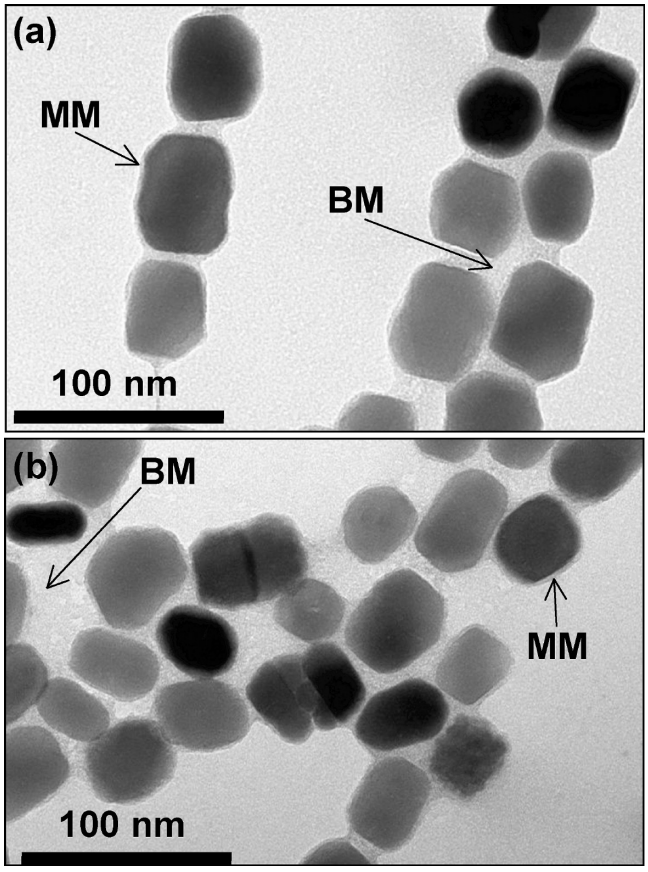


**Figure 6. TEM images of the extracted unheated magnetosomes (a) and extracted heated magnetosomes (b). The presence of the magnetosome membrane (MM) and biogenic material (BM) is shown in both cases.**

tracted magnetosomes comes from the difference in the compacity of the chains of magnetosomes. When the chains of magnetosomes are extracted from the bacteria, they form more compact assemblies increasing the dipolar interactions between them. To confirm the fact that the orientation of the magnetosome easy axes plays a minor role in the magnetic response, the extracted magnetosomes are treated to disrupt the remaining biological material, which binds the magnetosomes together, and to disorientate the magnetosome easy axes. To do so, the extracted magnetosomes are treated for 1 h at 90 °C in the presence of 1% of sodium dodecyl sulfate (SDS). The SDS-thermo treated extracted magnetosomes are then deposited on top of a TEM grid and on top of a silicon wafer using the same experimental protocol as that described previously for the extracted untreated magnetosomes. The TEM image shows that the extracted treated magnetosomes are also aligned forming a slightly more compact assembly (Figure 1e) than that observed with the extracted unheated magnetosomes (Figure 1c). Using the same approach as that described above, that is, by considering that the ⟨111⟩ crystallographic directions are determined by identifying the projected geometries, Figure 5c (enlarged regions of Figure 1e) shows that the majority of the magnetosomes do not have one of their ⟨111⟩ crystallographic direction orientated in the direction of the deposition field and therefore possess randomly orientated easy axes. In this case, the magnetosomes behave like individual nanoparticles. Hence their easy axes possess several possible orientations in the plane of the substrate. This creates a competing mechanism between the different easy axes orientated in different directions, which all try to align in the direction of the deposition field. Because of this competing mechanism, the easy axes of the extracted treated magnetosomes do not orientate in the direction of the deposition field. From that, it is concluded that the thermal treatment of the extracted magnetosomes in the presence of 1% SDS disrupts the biogenic material, which produces the alignment of the crystallographic planes and easy axes of the magnetosomes. To better understand the role played by the biogenic material in the alignment of the magnetosome easy axes, we show two TEM images of the extracted unheated (Figure 6a) and extracted heated (Figure 6b) magnetosomes. As can be seen in Figure 6a,b, the magnetosome membrane (MM) and the biogenic material (BM) binding the magnetosomes together are present in both samples. The presence of this material after heating and SDS treatment prevents the total collapse of the magnetosomes in a compact clump, which is expected after complete removal of all biogenic material and magnetosome membrane.[16,18,26] The disorientation of the magnetosome easy axes is a subtle effect, which may be due to the inactivation of a few specific proteins or enzymes, which can not easily be identified by TEM measurements.[27−30] To assess the magnetic properties of the extracted heated magnetosomes, the latter are deposited on a silicon substrate. As observed on the carbon grid, the SDS-thermo-treated magnetosomes also orientate on top of a silicon substrate (Figure 1f). The magnetic properties are similar to those observed with the extracted unheated magnetosome. Figure 2c shows a squarer hysteresis loop when the magnetic field is applied parallel to the oriented magnetosomes than when it is applied perpendicular to this direction. However, compared with the extracted unheated magnetosomes, the hysteresis loop is less square in the parallel field configuration (green line), while it remains identical in the perpendicular field configuration (red line). The values of $\Delta_{Mr/Ms}$ and $\Delta_{Hc}$ decrease from 80% and 50% for the extracted unheated magnetosomes down to 65% and 30% for the extracted heated ones. To determine if this decrease can be attributed to a loss of dipolar interactions, we estimate the ratio between the magnetostatic and anisotropy energies in this sample. Since the chains of magnetosomes have been destroyed, only single magnetosomes remain in this sample with a random orientation of their easy axes. Therefore, we estimate the magnetostatic energy between two single magneto-

somes, having a random orientation of their dipole. The latter lies between *ca.* $-2(V_M M_s)^2/4\pi a^3 \approx -8.2 \times 10^{-9}$ erg and *ca.* $(V_M M_s)^2/4\pi a^3 \approx 4.1 \times 10^{-9}$ erg, where $V_M \approx 2.7 \times 10^{-17}$ cm$^3$ is the volume of a single magnetosome, $M_s \approx 390$ emu/cm$^3$ is the saturation magnetization of maghemite, and $a \approx 3$ nm is the distance separating two magnetosomes. This yields a mean magnetostatic energy of $\langle E_{ms} \rangle \approx -2 \times 10^{-9}$ erg. Using the anisotropy energy of a single magnetosome, $E_k \approx 32 \times 10^{-13}$ erg, we deduce that $|\langle E_{ms} \rangle|/E_k \approx 625$. The value of $|\langle E_{ms} \rangle|/E_k$ is much larger than 1 indicating the presence of strong dipolar interactions between the magnetosomes in this sample. Compared with the extracted unheated magnetosomes, $|\langle E_{ms} \rangle|/E_k$ is slightly lower. Therefore, the loss of magnetic anisotropy between the extracted unheated and extracted heated magnetosomes has to arise either from a loss of dipolar interactions between the magnetosomes or from the disorientation of the magnetosome easy axes. These results clearly show the small influence of the alignment of the magnetosome easy axes on the magnetic anisotropy. Indeed, if there were such an influence, we would observe a strong decrease of $\Delta_{Hc}$ and $\Delta_{Mr/Ms}$ between the sample containing the extracted unheated magnetosomes and that containing the extracted heated magnetosomes. This is not the case.

Here, we conclude that the magnetic anisotropy of an assembly of aligned magnetosomes is mainly governed by the dipolar interactions between them and includes a smaller contribution, which is due to the alignment of their easy axes. From our knowledge, it is the first time that it is possible to explain the origin of the magnetic anisotropy in a system of aligned magnetic nanoparticles and to differentiate between the two contributions, that is, the nanoparticle dipolar interactions and the orientation of the nanoparticle easy axes. The dominant contribution of the dipolar interactions might arise from the large sizes of the magnetosomes of 20−50 nm for the majority of them.[9] Indeed, the magnetostatic energy, which measures the strength of these interactions, is proportional to the square volume of a magnetosome and is therefore strongly enhanced in a system of magnetic nanoparticles as large as the magnetosomes.

## METHODS

The AMB-1 magnetotactic bacteria are purchased from the ATCC (ATCC 700274). The solvent used for the preparation of the growth medium and the different samples is always water. The bacteria are cultivated in the growth medium recommended by the ATCC. The culture medium contains 1 L of distilled water in which are added in this order 5 mL of ATCC trace mineral supplement, 10 mL of ATCC vitamin supplement, 2 ml of a ferric quinate solution, 0.45 ml of 0.1% resazurin, 0.68 g of $KH_2PO_4$, 0.12 g of $NaNO_3$, 0.035 g of ascorbic acid, 0.37 g of tartaric acid, 0.37 g of succinic acid, and 0.05 g of sodium acetate. The ATCC vitamin supplement solution (ATCC MD-VS) is prepared by adding to 1 L of distilled water 2 mg of folic acid, 10 mg of pyridoxine hydrochloride, 5 mg of riboflavin, 2 mg of biotin, 5 mg of thiamine, 5 mg of nicotinic acid, 5 mg of pantothenic acid, 0.1 mg of vitamin B12, 5 mg of *p*-aminobenzoic acid, 5 mg of thioctic acid, and 900 mg of monopotassium phosphate. The solution of mineral supplement (ATCC MD-TMS) is prepared by adding to 1 L of distilled water 0.5 g of EDTA, 3 g of $MgSO_4 \cdot 7H_2O$, 0.5 g of $MnSO_4 \cdot H_2O$, 1 g of NaCl, 0.1 g of $FeSO_4 \cdot 7H_2O$, 0.1 g of $Co(NO_3)_2 \cdot 6H_2O$, 0.1 g of $CaCl_2$ (anhydrous), 0.1 g of $ZnSO_4 \cdot 7H_2O$, 0.01 g of $CuSO_4 \cdot 5H_2O$, 0.01 g of $AlK(SO_4)_2$ (anydrous), 0.01 g of $H_3BO_3$, 0.01 g of $Na_2MoO_4 \cdot 2H_2O$, 0.001 g of $Na_2SeO_3$ (anhydrous), 0.01 g of $Na_2WO_4 \cdot 2H_2O$ and 0.02 g of $NiCl_2 \cdot 6H_2O$. The ferric quinate solution is prepared by adding to 100 mL of distilled water 0.27 g of $FeCl_3$ and 0.19 g of quinic acid. After having added the chemicals given above, the pH of the growth medium is adjusted to 6.75 using a 1 M NaOH solution. The growth medium is autoclaved at 121 °C for 15 min. The bacteria provided by the ATCC are warmed up to room temperature and inserted in the growth medium under aseptic conditions. During their growth, the bacteria are kept at room temperature for one week until a change in the coloration of the growth medium is observed (from pink to white). A notice is available from the ATCC, which gives a detailed explanation of how to cultivate these bacteria.

The cells are harvested at stationary phase and three different types of samples are prepared. The living bacteria are first centrifugated at 8000 rpm for 15 min. The solution is then placed against a magnet and the supernatant containing the growth medium is removed and replaced by 3 mL of deionized water. Hence, we obtain 3 mL of a solution of whole bacteria dispersed in water, which we divide in three separated ependorphs of 1 mL. The first solution is not treated further. It simply contains 1 mL of whole bacteria and is used to study the properties of the whole bacteria. The solution contained in the second ependorph is redispersed in a 10 mM Tris buffer and sonicated during 20 min at 30 W to extract the chains of magnetosomes from the whole bacteria. After sonication, the solution containing the extracted chains of magnetosomes is placed against a magnet and the supernatant is removed to get rid of most of the biogenic material. The solution is washed 10 times in this way. It is designated as the solution of extracted unheated magnetosomes. The solution contained in the third ependorph is prepared by first following the same method as that used to prepare the second solution. It is then heated for 1 h at 90 °C in the presence of 1% SDS. The solution contained inside the ependorph is heated by placing the ependorph inside boiling water. The third solution is designated as the solution of extracted heated magnetosomes.

The three solutions containing the whole bacteria, the extracted unheated, and extracted heated magnetosomes are deposited on top of a carbon grid for TEM analysis and on top of a silicon substrate for SEM analysis and magnetic measurements. They are deposited in the presence of a magnetic field of either 0.2 T (extracted unheated and extracted heated magnetosomes) or 1 T (whole bacteria). The strengths of the magnetic fields used correspond to those which produced the strongest magnetic anisotropy. During the solvent evaporation, the substrates are placed between the two poles of a magnet, which produces a uniform magnetic field. The volumes deposited on top of the TEM grids and silicon substrates are 10 and 50 μL, respectively. The percentages in weight of maghemite of the different solutions deposited on top of the TEM grids are *ca.* $2 \times 10^{-5}$ % for the whole bacteria, *ca.* $2 \times 10^{-4}$ % for the extracted unheated magnetosomes, and $4 \times 10^{-5}$ % for the extracted heated magnetosomes. For the deposition on top of the silicon substrate, the same percentages as those above are used for SEM analysis, while 10 times more concentrated solutions are used for the magnetic measurements.

A JEOL (100 kV) model JEM 1011 transmission electron microscope (TEM) is used to obtain low-magnification micrographs of the magnetosomes and magnetotactic bacteria. The high-resolution transmission electron microscopy (HRTEM) images are recorded by using a JEOL 4000EX, which is operated at 400 kV and has a point-to-point resolution around 0.17 nm. The as-

semblies of magnetosomes are imaged with a JEOL model JSM-5510LV scanning electron microscope. A VSM (vibrating sample magnetometer) from Quantum design is used to perform the magnetic measurements. The samples are placed inside a capsule and hysteresis loops are carried out at a series of different temperatures ranging from 10 up to 300 K. In these measurements, the response of the capsule is subtracted from that of the sample by measuring the response of a blank sample in which the magnetosomes are absent. The hysteresis loops are measured between −2 and 2 T, magnetic field intensities, which exceeds those necessary to saturate the samples (0.1−0.2 T).

The percentage in weight of maghemite in the different solutions is determined by depositing 50 μL of each of the three solutions studied (containing either the whole bacteria, the extracted unheated magnetosomes, or the extracted heated magnetosomes) on top of a silicon substrate. We compare the value of the saturating magnetization of the different samples with that of maghemite (390 emu/cm$^3$) to estimate the percentage in weight of maghemite in the different solutions. Since the different solutions studied have a very similar weight as that of water, their percentages in weight are estimated relatively to the specific weight of water.

The composition of the magnetosomes is determined using SIRM (saturating isothermal remanent magnetization) following a method described in a previous report.[9] Briefly, the samples are cooled down in the presence of a 2.5 T magnetic field. The magnetic field is then switched of and the magnetization is measured as a function of increasing temperature from 10 up to 300 K. The absence of the Verwey transition in the SIRM spectra reveals the oxidation of the magnetosomes into maghemite. This technique is standard and introduced in reference.[31]

Finally, note that although previous studies reported that AMB-1 cells possess a single long chain of magnetosomes,[32,33] we repeatedly observe that under the conditions used in our study, the magnetosomes arrange in aligned short chains. This variation in the experimental conditions is taken into account to analyze the data of this study.

*Supporting Information Available:* Supplementary figures. This material is available free of charge *via* the Internet at http://pubs.acs.org.

## REFERENCES AND NOTES


1. Parekh, V.; Chunsheng, E.; Smith, D.; Ruiz, A.; Wolfe, J. C.; Ruchhoeft, P.; Svedberg, E.; Khizroev, S.; Litvinov, D. Fabrication of a High Anisotropy Magnetic Recording Device for Data Storage Application. *Nanotechnology* **2006**, *17*, 2079–2082.
2. Sun, X.; Huang, Y.; Nikles, D. E. FePt and CoPt Magnetic Nanoparticles Film for Future High Density Data Storage Media. *Int. J. Nanotechnol.* **2004**, *1*, 328–346.
3. Stoner, E. C.; Wohlfarth, E. P. A Mechanism of Magnetic Hysteresis in Heterogenous Alloys. *Philos. Trans. R. Soc. London, Ser. A* **1991**, *27*, 3475.
4. Russier, V.; Petit, C.; Pileni, M. P. Hysteresis Curve of Magnetic Nanocrystals Monolayers: Influence of the Structure. *J. Appl. Phys.* **2003**, *93*, 10001–10010.
5. Sahoo, Y.; Cheon, M.; Wang, S.; Luo, H.; Furlani, E., P.; Prasard, P. N. Field-Directed Self-Assembly of Magnetic Nanoparticles. *J. Phys. Chem. B* **2004**, *108*, 3380–3383.
6. Ngo, A. T.; Pileni, M. P. Nanoparticles of Cobalt Ferrite: Influence of the Applied Field on the Organization of the Nanocrystals on a Substrate and on Their Magnetic Properties. *Adv. Mater.* **2000**, *12*, 276–279.
7. Pileni, M. P. Magnetic Fluids: Fabrication, Magnetic Properties, and Organization of Nanocrystals. *Adv. Funct. Mater.* **2001**, *11*, 323–336.
8. Bazylinski, D. A.; Frankel, R. B. Magnetosome Formation in Prokaryotes. *Nat. Rev. Microbiol.* **2004**, *2*, 217–230.
9. Alphandéry, E.; Ngo, A. T.; Lefèvre, C.; Lisiecki, I.; Wu, L. F.; Pileni, M.-P. Difference Between the Magnetic Properties of the Magnetotactic Bacteria and Those of the Extracted Magnetosomes: Influence of the Distance Between the Chains of Magnetosomes. *J. Phys. Chem. C* **2008**, *112*, 12304–12309.
10. Posfai, M.; Kasama, T.; Dunin-Borkowski, R. E. Characterization of Bacterial Magnetic Nanostructures Using High-Resolution Transmission Electron Microscopy and Off-Axis Electron Holography. *Microbiol. Monogr.* **2007**, *3*, 197–225.
11. Dunin-Borkowski, R. E.; McCartney, M. R.; Posfai, M.; Frankel, R. B.; Bazylisnki, D. A.; Buseck, P. R. Off-Axis Electron Holography of Magnetotactic Bacteria: Magnetic Microstructure of Strains MV-1 and MS-1. *Eur. J. Miner.* **2001**, *13*, 671–684.
12. Dunin-Borkowski, R. E.; McCartney, M. R.; Frankel, R. B.; Bazylinski, D. A.; Posfai, M.; Buseck, P. R. Magnetic Microstructure of Magnetotactic Bacteria by Electron Holography. *Science* **1998**, *282*, 1868–1870.
13. Thomas, J. M.; Simpson, E. T.; Kasana, T.; Dunin-Borkowski, R. E. Electron Holography for the Study of Magnetic Nanomaterials. *Acc. Chem. Res.* **2008**, *41*, 665–674.
14. Komeili, A.; Li, Z.; Newman, D., K.; Jensen, G. J. Magnetosomes Are Cell Membrane Invaginations Organized by the Actin-like Protein MamK. *Science* **2006**, *311*, 242–245.
15. Pradel, N.; Santini, C.; L.; Bernadac, A.; Fukumori, Y.; Wu, L. F. Biogenesis of Actin-like Bacterial Cytoskeletal Filaments Destined for Positioning Prokaryotic Magnetic Organelles. *Proc. Natl. Acad. Sci. U.S.A.* **2006**, *103*, 17485–17489.
16. Scheffel, A.; Gruska, M.; Faivre, D.; Linaroudis, A.; Plitzko, J., M.; Schüler, D. An Acidic Protein Aligns Magnetosomes along a Filamentous Structure in Magnetotactic Bacteria. *Nature* **2006**, *440*, 110–114.
17. Chen, A. P.; Egli, R.; Moskowitz, B. M. First-Order Reversal Curve (FORC) Diagrams of Natural and Cultured Biogenic Magnetic Particles. *J. Geophys. Res. Solid Earth* **2007**, *112*, B08S90.
18. Kobayashi, A.; Kirschvink, J. L.; Nash, C. Z.; Kopp, R. E.; Sauer, D. A.; Bertani, L. E.; Voorhout, W. F.; Taguchi, T. Experimental Observation of Magnetosome Chain Collapse in Magnetotactic Bacteria: Sedimentological, Paleomagnetic, and Evolutionary Implications. *Earth Planet. Sci. Lett.* **2006**, *245*, 538–550.
19. Pan, Y.; Peterson, N.; Winklhofer, M.; Davila, A, F.; Liu, Q.; Frederichs, T.; Hanzlik, M.; Zhu, R. Rock Magnetic Properties of Uncultured Magnetotactic Bacteria. *Earth Planet. Sci. Lett.* **2005**, *237*, 311–325.
20. Majetich, S. A.; Sachan, M. Magnetostatic Interactions in Magnetic Nanoparticle Assemblies: Energy, Time and Length Scale. *J. Phys. D: Appl. Phys.* **2006**, *39*, R407−R422.
21. Farrell, D.; Cheng, Y.; McCallum, W.; Sachan, M.; Majetich, S. A. Magnetic Interactions of Iron Nanoparticles in Arrays and Dilute Dispersions. *J. Phys. Chem. B* **2005**, *109*, 13409–13419.
22. Taoka, A.; Asada, R.; Wu, L.-F.; Fukumori, Y. Polymerization of the Actin-like Protein MamK, Which Is Associated with Magnetosomes. *J. Bacteriol.* **2007**, *189*, 8737–8740.
23. Thomas-Keprta, K. L.; Bazylinski, D., A.; Kirschvink, J., L.; Clemett, S., J.; McKay, D. S.; Wentworth, S., J.; Vali, H.; Gibson, E., K.; Romanek, C., S. Elongated Prismatic Magnetite Crystals in ALH84001 Carbonate Globules: Potential Martian Magnetofossils. *Geochim. Cosmochim. Acta* **2000**, *64*, 4049–4081.
24. Kirschvink, J. L.; Kobayashi-Kirschvink, A.; Woodford, B. J. Magnetite Biomineralization in the Human Brain. *Proc. Natl. Acad. Sci.U.S.A.* **1992**, *89*, 7683–7687.
25. Devouard, B.; Posfai, M.; Hua, X.; Bazylinski, D., A.; Frankel, R. B.; Buseck, P., R. Magnetite from Magnetotactic Bacteria: Size Distribution and Twinning. *Am. Mineral.* **1998**, *83*, 1387–1398.
26. Faivre, D.; Schüler, D. Magnetotactic Bacteria and Magnetosomes. *Chem. Rev.* **2008**, *11*, 4875–4898.
27. Schüler, D. Molecular Analysis of a Cellular Compartment: The Magnetosome Membrane in *Magnetospirillum gryphiswaldense*. *Arch. Microbiol.* **2004**, *181*, 1–7.
28. Arakaki, A.; Webb, J.; Matsunaga, T. A Novel Protein Tightly Bound to Bacterial Magnetic Particles in *Magnetospirillum Magneticum* Strain AMB-1. *J. Biol. Chem.* **2003**, *278*, 8745–8750.

29. Komeili, A.; Vali, H.; Beveridge, T. J.; Newman, D. K. Magnetosome Vesicles Are Present before Magnetite Formation, and MamA Is Required for Their Activation. *Proc. Natl. Acad. Sci. U.S.A.* **2004**, *101*, 3839–3844.
30. Okamura, Y.; Takeyama, H.; Matsunaga, T. A Magnetosome-Specific GTPase from the Magnetic Bacterium *Magnetospirillum Magneticum* AMB-1. *J. Biol. Chem.* **2001**, *276*, 48183–48188.
31. Moskowitz, B. M.; Frankel, R. B.; Bazylinski, D. A. Rock Magnetic Criteria for the Detection of Biogenic Magnetite. *Earth Planet. Sci. Lett.* **1993**, *120*, 283–300.
32. Komeili, A. Molecular Mechanisms of Magnetosome Formation. *Annu. Rev. Biochem.* **2007**, *76*, 351–366.
33. Matsunaga, T.; Okamura, Y. Genes and Proteins Involved in Bacterial Magnetic Particle Formation. *Trends Microbiol.* **2003**, *11*, 536–541.